MELiSSA

T E C H N I C A L N O T E

Memorandum of Understanding TOS-MCT/2002/3161/In/CL

TECHNISCHE UNIVERSITÄT HAMBURG-HARBURG

biotechnologie

TECHNICAL NOTE: 3.6

DETERMINATION OF REACTOR STABILITY AND ENERGY REQUIREMENTS OF THE HYPERTHERMOPHILIC DIALYSIS REACTOR

prepared by/*préparé par* Jürgen Kube

reference/*réference* 14719/00/NL/SH
issue/*édition* 1
revision/*révision* 0
date of issue/*date d'édition* Oct. 15th 2004
status/*état* Draft
Document type/*type dedocument* Technical Note
Distribution/*distribution*

C O N F I D E N T I A L D O C U M E N T

A P P R O V A L

Title *titre*	issue 1 *issue*	revision 0 *revision*

author *auteur*	date *date*

approved by *approuvé by*	date *date*

C H A N G E L O G

reason for change /*raison du changement*	issue/*issue*	revision/*revision*	date/*date*

C H A N G E R E C O R D

Issue: 1 Revision: 0

reason for change/*raison du changement*	page(s)/*page(s)*	paragraph(s)/*paragraph(s)*

TABLE OF CONTENTS

1 INTRODUCTION

The aim of the MAP project “A total converting and biosafe liquefaction compartment for MELiSSA” is to find alternative technologies to improve the MELiSSA liquefaction process. Our part in the project is the application of hyperthermophilic anaerobic microorganisms to improve and speed up the liquefaction process.

The degradation velocity and thus the size of the liquefaction loop is an important parameter. Large liquefaction bioreactors will lead to reduced scientific payload in future space applications. The first aim therefore was to reduce the reactor size and enhance the volumetric loading rate. Our idea is combining different reactors and separation apparatus rather than applying a simple batch or continuous reactor. This more complex system requires higher regulation demands but also offers the benefit of reduced weight.

Hyperthermophilic microorganisms offer many benefits in the liquefaction process. A lot of biopolymers can be degraded by extra cellular enzymes from hyperthermophiles. The solubility and bioavailability of polymers increases with temperature. The elevated temperature also prevents the growth and accumulation of human pathogenic microorganisms.

In the first phase of the project a hyperthermophilic consortium was isolated from hot springs from the Azores. The degradation of the ESA substrate was fast but incomplete in batch and continuous mode. In the beginning of the second phase of the project continuous dialysis experiments were done. The degradation rate was increased to more than 70%. High volumetric loading rates of 13 g/(L d) were realized. The hyperthermophilic reactor works as a liquefaction unit, no biogas is produced in reasonable amounts. For biosafety reasons the effluent has to be checked for toxic compounds or metabolites.

2 ANALYSIS OF REACTOR EFFLUENT

2.1 Materials and Methods

2.1.1 DOC

The DOC and TIC value of the samples was determined with TOC + TN_b from Analytic Jena. Part of the sample is burnt at 800°C in a pure oxygen atmosphere in a column filled with carriers of Cer catalyst. The CO_2 content in the off-gas is integrated and the total carbon (TC) determined. The Total Inorganic Carbon (TIC) is determined by acidifying the sample to pH 2 and flushing out the dissolved CO_2

2.1.2 VFA

VFA are determined with a headspace gas chromatograph Chrompack CP9001. A 30mx0.32mm Nukol capillary from Supelco is used. Carrier gas is nitrogen. The samples are acidified with 2% H_3PO_4. The column is heated to 60°C, after tree minutes the temperature rises with 10°C/min to 200°C. The detector is a FID working at 220°C. The following VFA can be measured: C2, C3, i-C4, n-C4, i-C5, n-C5, n-C6, n-C7

2.1.3 AMINO ACIDS

Amino acids are determined with HPLC analysis. The samples are derivated with OPA agent containing phthaldialdehyde, 2-mercaptoethanol and methanol in Borate buffer at pH 9.5. The detector was a fluorescence detector.

2.1.4 PROTEINS (LOWRY-ASSAY)

The Lowry assay uses the ability of proteins to form colored complexes with copper under alkaline conditions. A copper agent is prepared form the following solutions. 0.5mL K-Na-Tartrate (4% w/v), 0.5mL $CuSO_4$ (2% w/v) and 99mL Na_2CO_3 (3% w/v) are mixed and stored at 4°C for a maximum of two weeks. Folin-Ciocalteau agent is mixed with 50% demineralized water.
100µL Sample is added to 1mL copper agent and incubated at room temperature for 15 minutes. 100µL Folin agent are added afterwards. The mixture is incubated for another 30 minutes. The adsorption at 660nm is measured against a blind sample.
The protein content is calculated with the help of a calibration curve of 0.02-0.4g/L bovine serum albumin (BSA). All measurements are done in duplicate.

2.1.5 CARBOHYDRATES

Carbohydrates are determined by measuring the reducing sugars after acidic hydrolysis of the sample. Anthron solution is prepared from 200mg Anthron agent, dissolved in 5mL ethanol and filled up to 100 ml with 75% Sulphuric acid.
0.5mL Sample and 2 mL Anthron Solution are given into a cuvette and are incubated for 10 min at 100°C. The reaction is stopped on ice. The absorption at 635nm is measured against demineralized water. The carbohydrate content is calculated with a calibration curve made with 1% autoclaved starch solution. The test is valid between 5 and 100 mg/L. Samples with higher carbohydrate concentration are diluted with demineralized water.

2.1.6 REDUCED SUGARS

5g 2-Hydroxy-3,5-Dinitrobenzoic acid are dissolved in 100ml 2M NaOH. 250g Rochelle's salt are dissolved in 250ml demineralized water. Both solutions are poured together.
250µL of the DNS-solution are added to 500µL 0.05M Sodiumacetate buffer pH4.7. 250µL Sample is added. The mixture is incubated at 100°C for 5 minutes and cooled down on ice. The extinction is determined at 540nm. A calibration curve, done with glucose can be used to calculate the amount of reduced sugars. The test is valid from 0.05 to 3g/L glucose.

2.1.7 GC-MS

Gas chromatograph mass spectrometer analysis was used for qualitative non target screening. Samples were extracted 1:1 in dichloromethane. The detector was a Hewlett Packard.
Model HP 5971 A with GC-5890 Series II.

2.2 Results

Samples from reactor effluent and dialysate were examined. Quantitative analysis of protein, carbohydrates and their free monomers, amino acids and sugars were done. Volatile fatty acids were measured quantitatively. A qualitative non target screening for toxic substances was done by GS-MS analysis.
The results are listed in Table 1.

Table 1 Results from analysis of reactor effluent and dialysate. The dissolved organic carbon (DOC) concentration is given. The average carbon content (w/w) of sugar is 40%, of carbohydrates is 44%, and of protein is 46%. The proportions in percent are also given in figure 1

	Dialysate	Effluent
DOC [mg/L]	744.00	734.00
sugars [mg/L]	0.13	0.13
free AA [mg/L]	1.55	1.59
protein [mg/L]	310.53	335.18
VFA [mg/L]	82.51	149.85
carbohydrates [mg/L]	65.50	63.53
unknown [mg/L]	283.78	183.72

Both dialysate and effluent have similar concentration patterns. The largest group of soluble molecules is the protein fraction (46% effluent, 42% dialysate). The high concentration of protein in the dialysate is remarkable, because normally large protein do not diffuse through the membrane. However, throughout the fermentation often a convective stream over the membrane was monitored. The cut off of the membrane in ultra filtration mode is 300 kDa, so most of the proteins can be pressed through the membrane.
The second largest fraction is still unknown (25% effluent, 39% dialysate). Possible molecules are alcohols and aldehydes or non volatile fatty acids, like pyruvic or succinic acid.
The next fraction is the volatile fatty acid fraction (20% effluent, 11% dialysate), which consists mainly of acetic acid. Higher VFA (C3-C7) are just found in traces. Carbohydrates are found in both streams at the same concentration (9%). Free amino acids are just found in very small concentrations (0.2%). The same is valid for free sugars (0.02%).
Figure 1 gives a graphical overview over the found substances.
Besides quantitative determination a qualitative GC-MS analysis was done. The analysis revealed traces of alcanes and alcylamides in dialysate and effluent. These molecules or their precursors are natural degradation products of plant fibers [1]. Alcoholes, and fatty acids can be reduced enzymatically by Alcoholdehydrogenases (ADH) and Alcoholoxidoreductases (AOR) to alcanes. Microbial alkylamide formation was monitored in sewage sludge reactors [2].
In the dialysate also a peak was found, indicating the presence of a terpene. Terpenes are C_5-bodies, known as aromatic oils, but are neither oils nor aromatics.
No halogenated molecules were found in both streams. Halogens show a very characteristic isotropic pattern in the MS; this pattern was not found.
Aromatic molecules or arylgroups were not found as well.

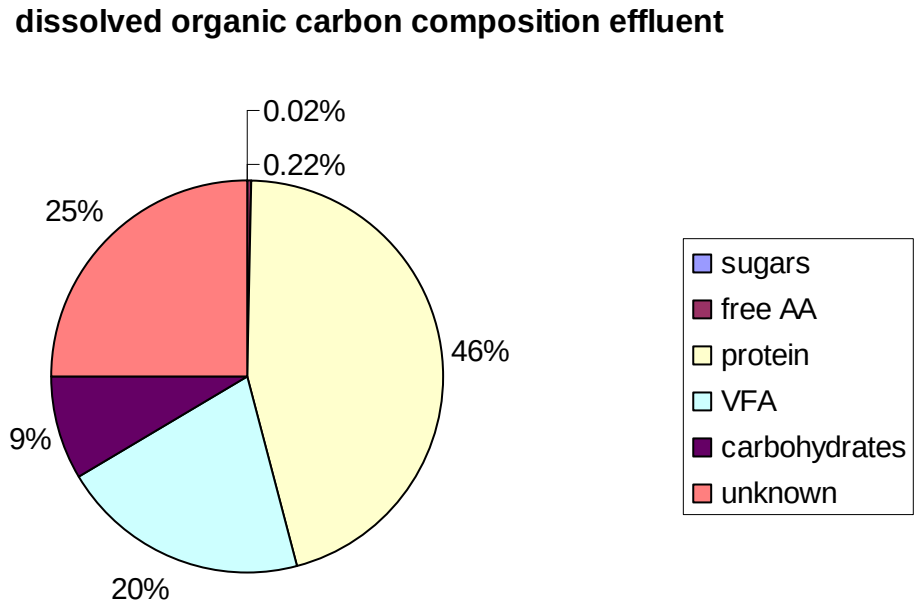

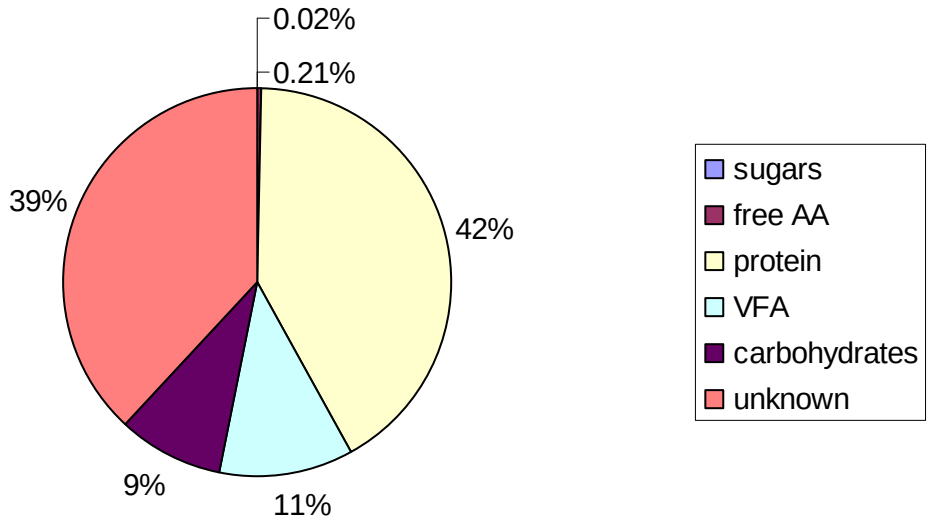

Figure 1 Moleculear composition of dissolved organic carbon for effluent (A) and dialysate (B) of hyperthermophilic fermentor

3 MATHEMATICAL MODELING OF LABORATORY REACTOR

To understand the liquefaction process in the hyperthermophilic dialysis reactor a simple mechanistic model was developed. The lab fermentor is shown in Figure 2

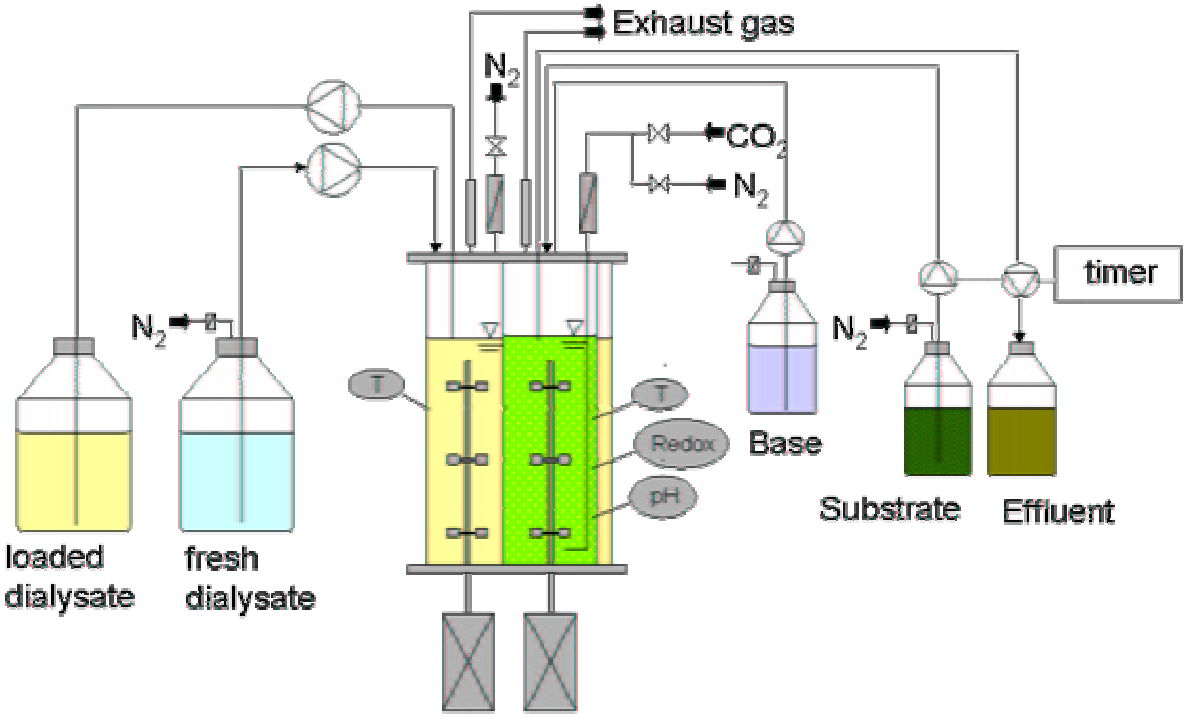

Figure 2 Lab-scale dialysis fermentor. The fermentor has a PES-dialysis membrane with an area of 5dm². Fresh dialysate is pumped continuously into the dialysate chamber. Substrate addition is triggered by a timer. pH is controlled online and maintained constant by addition of 2M NaOH.

The following assumptions are necessary:

- Solid particles are attacked by extra cellular enzymes and transformed into dissolved organic carbon (DOC) and volatile fatty acids (VFA).
- The liquefaction is a first order reaction.
- Biomass is not modeled
- Nitrogen is not modeled.
- Solid particles sediment in the fermentor. Only a small part of them will leave the fermentor with the effluent
- An average VFA molecule is balanced. VFA have similar behavior. (pK_{C2}=4.76, pK_{C3}=4.88, $pK_{i\text{-}C4}$=4.84, pK_{C4}= 4.82, pK_{C5+}=4.77)
- The production of CO_2 is neglected.

The following species are balanced:

Solid substrate, carbon content	s	[g/L]
DOC culture chamber	d_i	[g/L]

DOC dialysate chamber	d_o	[g/L]
VFA culture chamber	a_i	[g/L]
VFA dialysate chamber	a_o	[g/L]

The used indices are:

i	inner chamber (culture chamber)
o	outer chamber (dialysate chamber)
F	feed

System parameters:

DOC production coefficient	k_{DS}	[1/h]
VFA production coefficient	k_{AS}	[1/h]
Permeability DOC	P_D	[dm/h]
Permeability VFA	P_A	[dm/h]
Membrane area	A	[dm²]
Cultivation volume	V_i	[L]
Dialysate volume	V_o	[L]
Dilution rate cultivation chamber	D_i	[1/h]
Dilution rate dialysis chamber.	D_o	[1/h]
Sedimentation coefficient	β	[g/g]

The substrate balance is found in eq.1.

$$\frac{ds}{dt} = -(k_{as} + k_{ds})s + D_i(s_F - \beta \cdot s) \qquad \text{eq.1}$$

The DOC concentration in the culture chamber is written in eq.2.

$$\frac{dd_i}{dt} = k_{ds} \cdot s - D_i \cdot d_i - \frac{P_d A}{V_i}(d_i - d_o) \qquad \text{eq.2}$$

The DOC concentration in the outer chamber is shown in eq.3.

$$\frac{dd_o}{dt} = \frac{P_d A}{V_o}(d_i - d_o) - D_o \cdot d_o \qquad \text{eq.3}$$

The VFA concentration in the cultivation chamber is calculated according to eq.4.

$$\frac{da_i}{dt} = k_{as} \cdot s - D_i \cdot a_i - \frac{P_a A}{V_i}(a_i - a_o) \qquad \text{eq.4}$$

The VFA concentration in the dialysis chamber is depicted in eq.5.

$$\frac{da_o}{dt} = \frac{P_a A}{V_o}(a_i - a_o) - D_o \cdot a_o \qquad \text{eq.5}$$

The linear system is solved for stationary conditions by modifying the parameters. A Newton algorithm is used to fit the following parameters: k_{as}, k_{ds}, P_a, P_d, β.
The start point is
k_{as}=0.1 1/h
k_{ds}=1 1/h
P_a=0.05 dm/h

P_d=0.01 dm/h
β=0.1g/g
The input parameters are taken from an experiment.
s_F=4g/L, d_i=0.35g/L, d_o=0.1g/L, a_i=80mg/L, a_o=34mg/L, s=25.6g/L, V_i=1.5L, V_o=4.5L, A=5dm², D_i=0.01042 1/h, D_o=0.0833 1/h,
Eq.6 shows the linear system for stationary conditions.

$$\begin{pmatrix} -(k_{ds}+k_{as})-\beta\cdot D_i & 0 & 0 & 0 & 0 \\ k_{as} & -D_i-\frac{P_a A}{V_i} & \frac{P_a A}{V_i} & 0 & 0 \\ 0 & \frac{P_a A}{V_o} & -D_o-\frac{P_a A}{V_o} & 0 & 0 \\ k_{ds} & 0 & 0 & -D_i-\frac{P_d A}{V_i} & \frac{P_d A}{V_i} \\ 0 & 0 & 0 & \frac{P_d A}{V_o} & -D_o-\frac{P_d A}{V_o} \end{pmatrix} \cdot \begin{pmatrix} s \\ a_i \\ a_o \\ d_i \\ d_o \end{pmatrix} = \begin{pmatrix} -D_i\cdot s_F \\ 0 \\ 0 \\ 0 \\ 0 \end{pmatrix}$$

eq. 6.

The system is solved by multiplying the inverse matrix to the inhomogenity as shown in eq. 7

$$\vec{y} = A^{-1}\cdot\vec{b} \qquad \text{eq.7}$$

The solution leads to the indicated parameters.
k_{as}=0.00037 1/h
k_{ds}=0.00114 1/h
P_a=0.057 dm/h
P_d=0.030 dm/h
β=0.141g/g
With these parameters the scale up can be calculated (Chapter 4).
From the permeability the molar weight of an average VFA and DOC molecule can be estimated with the dependence of the permeability of a PES-membrane on the molar weight eq.8.

$$P\left[\frac{10^{-2}\,cm}{\min}\right] = 72\cdot\left(M\left[\frac{g}{mol}\right]\right)^{-0.86} \qquad \text{eq.8}$$

The average weight of a DOC molecule is 320g/mol. This is in the range of hexose dimer (342g/mol) or a pentose-hexose dimer (312g/mol). An average VFA molecule weights 150 g/mol (C8-VFA:144g/mol). The average VFA weight is higher than the expected value (M_{VFA}=66g/mol). The possible source of error is the convective stream over the membrane. In pure dialysis mode no convection appears. In this experimental setup a small convection flow was found from the cultivation chamber into the dialysate chamber.

4 MATHEMATICAL MODELING OF PILOT REACTOR

4.1 Construction of the model

The scale up of the laboratory reactor is necessary to circumvent huge dialysate vessels and large instable membrane areas. External dialysis modules supply large membrane areas within small volumes. Maintenance is also easier, because of the modular character of the system. Damaged membrane modules can be renewed without interrupting the liquefaction process. The pilot scale hyperthermophilic liquefaction unit will consist of four parts as shown in figure 3. The hyperthermophilic fermentor contains the biomass and the suspended solids. A micro filtration (MF) unit will separate the solid particles. A small part of the solid particles will be send to the *fibrobacter* unit; the larger part will be pumped back into the hyperthermophilic fermentor to increase the total solid concentration in the fermentor.
Solid free effluent is pumped through the dialysis module. The dialysis module is run in counter current mode. This mode supplies the lowest mass transport resistance. Fresh dialysate is supplied by the low pressure reverse osmosis (RO) unit. Here nutrients are separated from the dialysate. The RO-retentate will leave the liquefaction unit as highly concentrated nutrient stream.

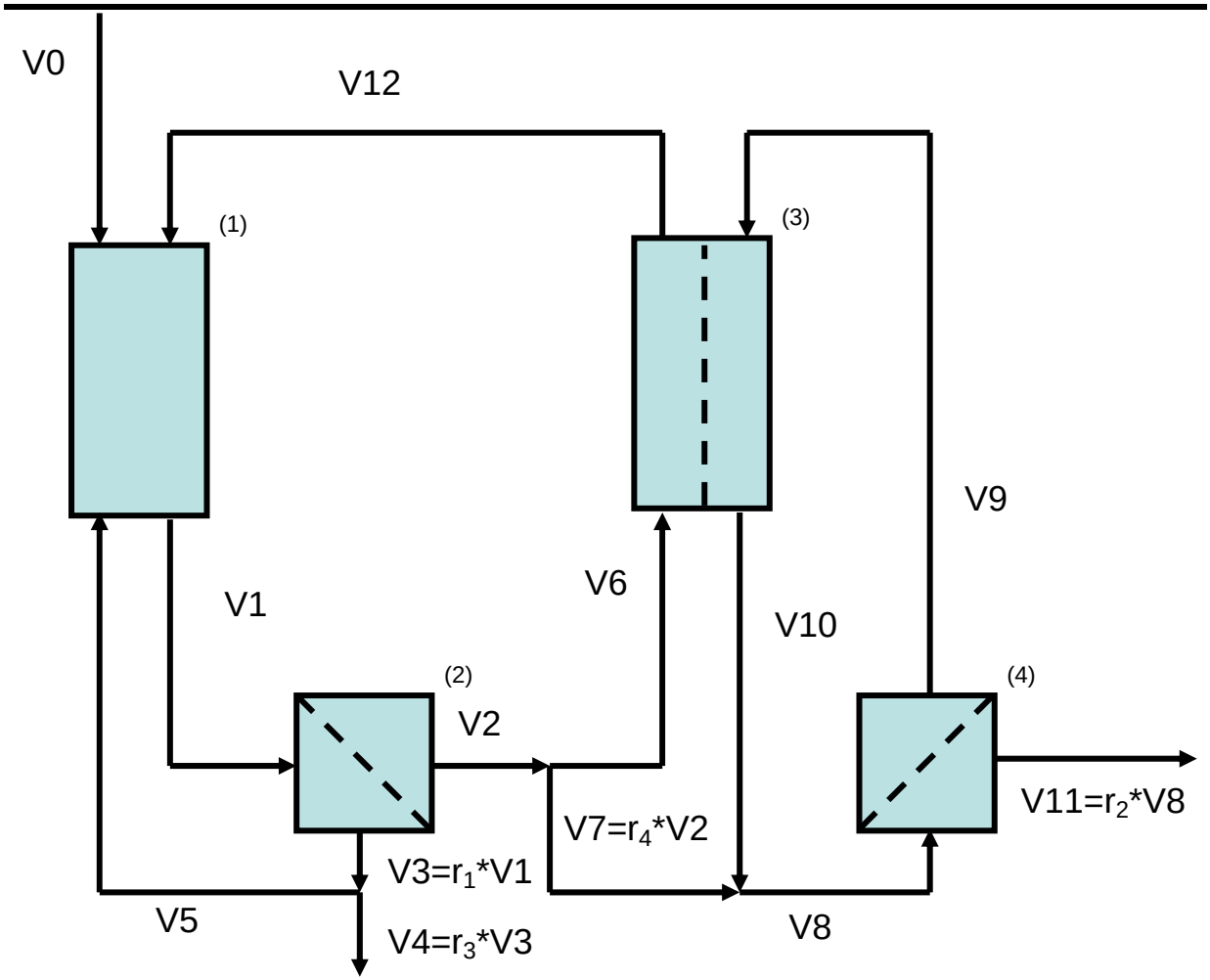

figure 3 reactor scheme of the hyperthermophilic liquefaction unit. (1) fermentor containing suspended solids and hyperthermophilic biomass. (2) MF separation unit. (3) PES dialysis module, run in counter current mode. (4) LP-RO unit

The system contains 13 mass streams. In four points a separation of a stream into two streams takes place. The distribution between the streams is described with the factors r1, r2, r3 and r4. If the distribution factors are given, the system is a linear 13x13 system (eq.9), which can be solved analytically.
Instead of setting the distribution coefficients four mass streams can be given. Then the distribution factors and the 9 other mass streams have to be calculated. In this case the system becomes non linear, but can nevertheless be solved. The solution is calculated numerically, using a Newton algorithm.

$$\begin{pmatrix} 0 & -r_4 & 0 & 0 & 0 & 0 & 1 & 0 & 0 & 0 & 0 & 0 & 0 \\ -1 & 0 & 0 & 0 & 1 & 0 & 0 & 0 & 0 & 0 & 0 & 1 & 1 \\ 1 & -1 & -1 & 0 & 0 & 0 & 0 & 0 & 0 & 0 & 0 & 0 & 0 \\ 0 & 0 & 1 & -1 & -1 & 0 & 0 & 0 & 0 & 0 & 0 & 0 & 0 \\ 0 & 1 & 0 & 0 & 0 & -1 & -1 & 0 & 0 & 0 & 0 & 0 & 0 \\ 0 & 0 & 0 & 0 & 0 & 0 & 1 & -1 & 0 & 1 & 0 & 0 & 0 \\ 0 & 0 & 0 & 0 & 0 & 0 & 0 & 1 & -1 & 0 & -1 & 0 & 0 \\ 0 & 0 & 0 & 0 & 0 & 0 & 0 & 0 & 1 & -1 & 0 & 0 & 0 \\ 0 & 0 & 0 & 0 & 0 & 1 & 0 & 0 & 0 & 0 & 0 & -1 & 0 \\ -r_1 & 0 & 1 & 0 & 0 & 0 & 0 & 0 & 0 & 0 & 0 & 0 & 0 \\ 0 & 0 & 0 & 0 & 0 & 0 & 0 & -r_2 & 0 & 0 & 1 & 0 & 0 \\ 0 & 0 & -r_3 & 1 & 0 & 0 & 0 & 0 & 0 & 0 & 0 & 0 & 0 \\ 0 & 0 & 0 & 0 & 0 & 0 & 0 & 0 & 0 & 0 & 0 & 0 & 1 \end{pmatrix} \bullet \begin{pmatrix} \dot{m}_1 \\ \dot{m}_2 \\ \dot{m}_3 \\ \dot{m}_4 \\ \dot{m}_5 \\ \dot{m}_6 \\ \dot{m}_7 \\ \dot{m}_8 \\ \dot{m}_9 \\ \dot{m}_{10} \\ \dot{m}_{11} \\ \dot{m}_{12} \\ \dot{m}_0 \end{pmatrix} = \begin{pmatrix} 0 \\ 0 \\ 0 \\ 0 \\ 0 \\ 0 \\ 0 \\ 0 \\ 0 \\ 0 \\ 0 \\ 0 \\ \dot{m}_{in} \end{pmatrix} \quad \text{(eq.9)}$$

In the next step the mass flows of the species solid particles (s), DOC (d) and VFA (a) are modeled. For each species the distribution coefficients have to be defined. This is shown in Table 2. The distribution coefficient r2 for DOC and VFA is typical for a low pressure RO-Unit. 99% of small molecules with a molecular weight of less than 100Da will be retained; bigger molecules will go through the membrane much slower thus resulting in a 99.9% retention.

Table 2 distribution coefficients of the species mass flows

Mass flow	Solid particle (s)	DOC (d)	VFA (a)
r1	1	=r1	=r1
r2	0	=1-0.001*Q_9/Q_8	=1-0.01*Q_9/Q_8
r3	=r3	=r3	=r3
r4	0	=r4	=r4

To describe the species mass flows a system similar to eq. 9 has to be solved for each species. Changes occur in row 2, 8 and 9.
Row 2 describes the mass balance over the fermentor. (eq.10)

$$-\dot{x}_1 + \dot{x}_5 + \dot{x}_{12} + \dot{x}_0 = 0 \qquad \text{(eq.10)}$$

For the substrate the mass balance is modified similar to eq.1 (eq.11)

$$\frac{ds}{dt} = 0 = \frac{-\dot{s}_1 + \dot{s}_5 + \dot{s}_{12} + \dot{s}_0}{m_1} - \left(k_{as} + k_{ds}\right) \cdot s_1 \qquad \text{(eq.11)}$$

This leads to eq.12.

$$0 = -\dot{s}_1 + \dot{s}_5 + \dot{s}_{12} + \dot{s}_0 - \left(k_{as} + k_{ds}\right) \cdot \dot{s}_1 \cdot \frac{m_1}{\dot{m}_1} \qquad \text{(eq.12)}$$

For DOC and VFA the mass balance is calculated with eq.13 and 14.

$$0 = -\dot{d}_1 + \dot{d}_5 + \dot{d}_{12} + \dot{d}_0 + k_{ds} \cdot \dot{s}_1 \cdot \frac{m_1}{\dot{m}_1} \quad \text{(eq.13)}$$

$$0 = -\dot{a}_1 + \dot{a}_5 + \dot{a}_{12} + \dot{a}_0 + k_{as} \cdot \dot{s}_1 \cdot \frac{m_1}{\dot{m}_1} \quad \text{(eq.14)}$$

The mass balances are all linear equations.
Row 8 and 9 describe the mass balance over the dialysate module. There is no transport of mass flows or the solid particles over the membrane. For DOC and VFA species the balances will be shown in eq.15 and eq.16.

$$\dot{x}_9 - \dot{x}_{10} = -PA \cdot \Delta x \quad \text{(eq.15)}$$

$$\dot{x}_6 - \dot{x}_{12} = +PA \cdot \Delta x \quad \text{(eq.16)}$$

for counter current the mean logarithmic concentration gradient is defined as in eq.17.

$$\Delta x = \frac{(x_{12} - x_9) - (x_6 - x_{10})}{\ln\left(\frac{x_{12} - x_9}{x_6 - x_{10}}\right)} \quad \text{(eq.17)}$$

With the introduction of the mean logarithmic gradient the system becomes non linear and thus harder to solve. To avoid non-linearities the mean logarithmic gradient can be linearized as shown in eq. 18.

$$\Delta x = \frac{(x_{12} - x_9) + (x_6 - x_{10})}{2} \quad \text{(eq.18)}$$

This simplification leads to great errors and sometimes to negative concentrations and species flows. The error can be minimized by splitting the module into a number of intersections. Within this intersections the mean logarithmic gradient can be linearized without great error. For the modeling of this system the module was split into tree sub modules as shown in figure 4. Later on the calculations showed that three sub modules are enough for moderate membrane areas up to 20m²/m³. For higher membrane areas more intersections will be reasonable. The error can be quantified by comparing the lineraized Δx with the logarithmic Δx. The error depends highly on the specific membrane area. Membrane areas up to 20m²/m³ yielded an error of up to 15%. Higher membrane areas will lead to higher errors. At very high membrane areas the concentrations at the intersection points can become negative. The addition of one intersection point will enlarge the matrix by 4 rows and 4 columns.
Attempts to solve the non linear equation system have been undergone in matlab and MS-Excel using a more dimensional Newtonian algorithm, which normally leads to good results. Both attempts failed. The reason for this lies probably in the nature of the logarithm function. The Newton-algorithm works by determining the tangent of the function at the starting point, calculating the crossing of the tangent with the abscissa and taking this value as next starting point. If the argument of the logarithm is greater than 1, the next iteration step leads to negative arguments.
The logarithm function is not defined for negative arguments, thus aborts any iteration loop
The linearized system has not to be solved numerically, but can be calculated analytically instead.

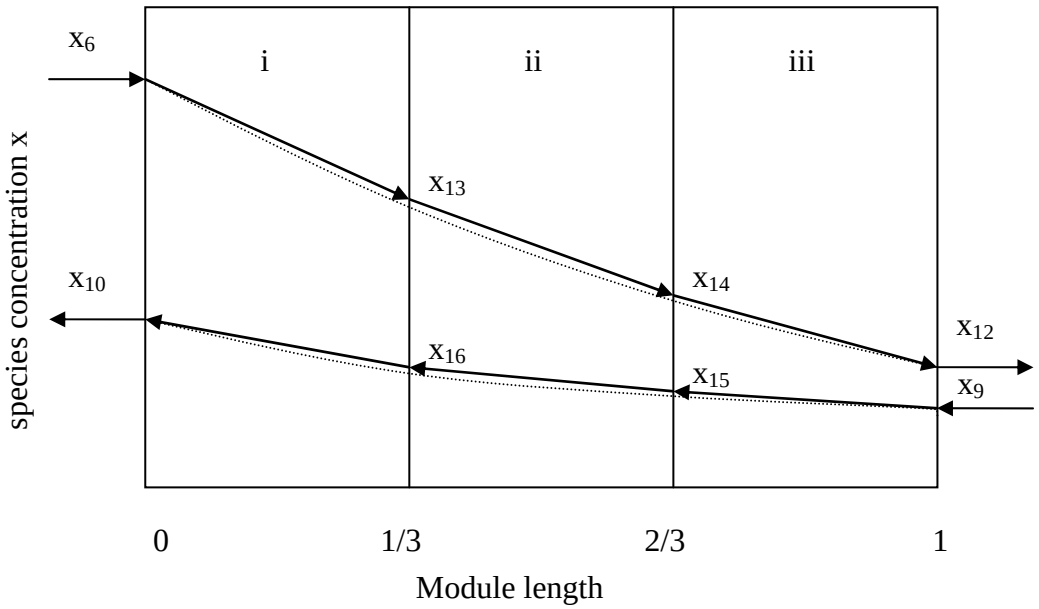

figure 4 linearization of the concentration gradient over the dialysis module in three intersection. Broad arrows indicate the linearization, dashed lines indicate the logarithmic concentration profile. The points 13-16 are new and can be calculated with linear equations.

The concentrations at the borders of the intersections are calculated with the following six equations. (eq.19-eq.24)

$$0 = -\left(1+\frac{PA}{6\cdot\dot{m}_{10}}\right)\dot{x}_{10} + \frac{PA}{6\cdot\dot{m}_{6}}\dot{x}_{13} + \frac{PA}{6\cdot\dot{m}_{6}}\dot{x}_{6} + \left(1-\frac{PA}{6\cdot\dot{m}_{10}}\right)\dot{x}_{16} \qquad \text{(eq.19)}$$

$$0 = -\left(1+\frac{PA}{6\cdot\dot{m}_{10}}\right)\dot{x}_{15} + \frac{PA}{6\cdot\dot{m}_{6}}\dot{x}_{13} + \frac{PA}{6\cdot\dot{m}_{6}}\dot{x}_{14} + \left(1-\frac{PA}{6\cdot\dot{m}_{10}}\right)\dot{x}_{16} \qquad \text{(eq.20)}$$

$$0 = -\left(1+\frac{PA}{6\cdot\dot{m}_{10}}\right)\dot{x}_{15} + \frac{PA}{6\cdot\dot{m}_{6}}\dot{x}_{12} + \frac{PA}{6\cdot\dot{m}_{6}}\dot{x}_{14} + \left(1-\frac{PA}{6\cdot\dot{m}_{10}}\right)\dot{x}_{9} \qquad \text{(eq.21)}$$

$$0 = -\left(1+\frac{PA}{6\cdot\dot{m}_{6}}\right)\dot{x}_{13} + \frac{PA}{6\cdot\dot{m}_{10}}\dot{x}_{16} + \frac{PA}{6\cdot\dot{m}_{10}}\dot{x}_{10} + \left(1-\frac{PA}{6\cdot\dot{m}_{6}}\right)\dot{x}_{6} \qquad \text{(eq.22)}$$

$$0 = -\left(1+\frac{PA}{6\cdot\dot{m}_{6}}\right)\dot{x}_{14} + \frac{PA}{6\cdot\dot{m}_{10}}\dot{x}_{16} + \frac{PA}{6\cdot\dot{m}_{10}}\dot{x}_{15} + \left(1-\frac{PA}{6\cdot\dot{m}_{6}}\right)\dot{x}_{13} \qquad \text{(eq.23)}$$

$$0 = -\left(1+\frac{PA}{6\cdot\dot{m}_{6}}\right)\dot{x}_{12} + \frac{PA}{6\cdot\dot{m}_{10}}\dot{x}_{9} + \frac{PA}{6\cdot\dot{m}_{10}}\dot{x}_{15} + \left(1-\frac{PA}{6\cdot\dot{m}_{6}}\right)\dot{x}_{14} \qquad \text{(eq.24)}$$

The first two equations replace row 8 and 9 in the matrix, the last four equations are attached to the system. So in total 46 linear equations have to be solved. The linear system is shown in equation 25.

$$\begin{pmatrix} A_{11} & 0_{(13x13)} & 0_{(13x13)} & 0_{(13x8)} & 0_{(13x8)} \\ A_{21} & A_{22} & 0_{(13x13)} & A_{24} & 0_{(13x8)} \\ A_{31} & 0_{(13x13)} & A_{33} & 0_{(13x8)} & A_{35} \\ & 0_{(8x13)} & B_{(8x39)} & & \end{pmatrix} \cdot \begin{pmatrix} s \\ d \\ a \\ b \end{pmatrix} = \begin{pmatrix} s_0 \\ 0 \\ 0 \\ 0 \end{pmatrix} \qquad \text{(eq.25)}$$

with

$$A_{11} = \begin{pmatrix} 0 & -r_4 & 0 & 0 & 0 & 0 & 1 & 0 & 0 & 0 & 0 & 0 & 0 \\ -1 & 0 & 0 & 1 & 0 & 0 & 0 & 0 & 0 & 0 & 0 & 1 & 1 \\ 1 & -1 & -1 & 0 & 0 & 0 & 0 & 0 & 0 & 0 & 0 & 0 & 0 \\ 0 & 0 & 1 & -1 & -1 & 0 & 0 & 0 & 0 & 0 & 0 & 0 & 0 \\ 0 & 1 & 0 & 0 & 0 & -1 & -1 & 0 & 0 & 0 & 0 & 0 & 0 \\ 0 & 0 & 0 & 0 & 0 & 0 & 1 & -1 & 0 & 1 & 0 & 0 & 0 \\ 0 & 0 & 0 & 0 & 0 & 0 & 0 & 1 & -1 & 0 & -1 & 0 & 0 \\ 0 & 0 & 0 & 0 & 0 & 0 & 0 & 0 & 1 & -1 & 0 & 0 & 0 \\ 0 & 0 & 0 & 0 & 0 & 1 & 0 & 0 & 0 & 0 & 0 & -1 & 0 \\ -r_1 & 0 & 1 & 0 & 0 & 0 & 0 & 0 & 0 & 0 & 0 & 0 & 0 \\ 0 & 0 & 0 & 0 & 0 & 0 & 0 & -r_2 & 0 & 0 & 1 & 0 & 0 \\ 0 & 0 & -r_3 & 1 & 0 & 0 & 0 & 0 & 0 & 0 & 0 & 0 & 0 \\ 0 & 0 & 0 & 0 & 0 & 0 & 0 & 0 & 0 & 0 & 0 & 0 & 1 \end{pmatrix}$$

$$A_{22} = \begin{pmatrix} 0 & -r_{d4} & 0 & 0 & 0 & 0 & 1 & 0 & 0 & 0 & 0 & 0 & 0 \\ -1 & 0 & 0 & 1 & 0 & 0 & 0 & 0 & 0 & 0 & 0 & 1 & 1 \\ 1 & -1 & -1 & 0 & 0 & 0 & 0 & 0 & 0 & 0 & 0 & 0 & 0 \\ 0 & 0 & 1 & -1 & -1 & 0 & 0 & 0 & 0 & 0 & 0 & 0 & 0 \\ 0 & 1 & 0 & 0 & 0 & -1 & -1 & 0 & 0 & 0 & 0 & 0 & 0 \\ 0 & 0 & 0 & 0 & 0 & 0 & 1 & -1 & 0 & 1 & 0 & 0 & 0 \\ 0 & 0 & 0 & 0 & 0 & 0 & 0 & 1 & -1 & 0 & -1 & 0 & 0 \\ 0 & 0 & 0 & 0 & 0 & \frac{P_d A}{6\dot{m}_6} & 0 & 0 & 0 & -\left(1+\frac{P_d A}{6\dot{m}_{10}}\right) & 0 & 0 & 0 \\ 0 & 0 & 0 & 0 & 0 & 0 & 0 & 0 & 0 & 0 & 0 & 0 & 0 \\ -r_{d1} & 0 & 1 & 0 & 0 & 0 & 0 & 0 & 0 & 0 & 0 & 0 & 0 \\ 0 & 0 & 0 & 0 & 0 & 0 & 0 & -r_{d2} & 0 & 0 & 1 & 0 & 0 \\ 0 & 0 & -r_{d3} & 1 & 0 & 0 & 0 & 0 & 0 & 0 & 0 & 0 & 0 \\ 0 & 0 & 0 & 0 & 0 & 0 & 0 & 0 & 0 & 0 & 0 & 0 & 1 \end{pmatrix}$$

$$A_{33} = \begin{pmatrix} 0 & -r_{a4} & 0 & 0 & 0 & 0 & 1 & 0 & 0 & 0 & 0 & 0 & 0 \\ -1 & 0 & 0 & 1 & 0 & 0 & 0 & 0 & 0 & 0 & 0 & 1 & 1 \\ 1 & -1 & -1 & 0 & 0 & 0 & 0 & 0 & 0 & 0 & 0 & 0 & 0 \\ 0 & 0 & 1 & -1 & -1 & 0 & 0 & 0 & 0 & 0 & 0 & 0 & 0 \\ 0 & 1 & 0 & 0 & 0 & -1 & -1 & 0 & 0 & 0 & 0 & 0 & 0 \\ 0 & 0 & 0 & 0 & 0 & 0 & 1 & -1 & 0 & 1 & 0 & 0 & 0 \\ 0 & 0 & 0 & 0 & 0 & 0 & 0 & 1 & -1 & 0 & -1 & 0 & 0 \\ 0 & 0 & 0 & 0 & 0 & \frac{P_a A}{6\dot{m}_6} & 0 & 0 & 0 & -\left(1+\frac{P_a A}{6\dot{m}_{10}}\right) & 0 & 0 & 0 \\ 0 & 0 & 0 & 0 & 0 & 0 & 0 & 0 & 0 & 0 & 0 & 0 & 0 \\ -r_{a1} & 0 & 1 & 0 & 0 & 0 & 0 & 0 & 0 & 0 & 0 & 0 & 0 \\ 0 & 0 & 0 & 0 & 0 & 0 & 0 & -r_{a2} & 0 & 0 & 1 & 0 & 0 \\ 0 & 0 & -r_{a3} & 1 & 0 & 0 & 0 & 0 & 0 & 0 & 0 & 0 & 0 \\ 0 & 0 & 0 & 0 & 0 & 0 & 0 & 0 & 0 & 0 & 0 & 0 & 1 \end{pmatrix}$$

$$A_{21} = \begin{pmatrix} 0 & 0 & 0 & 0 & 0 & 0 & 0 & 0 & 0 & 0 & 0 & 0 & 0 \\ \frac{m_1 k_{ds}}{\dot{m}_1} & 0 & 0 & 0 & 0 & 0 & 0 & 0 & 0 & 0 & 0 & 0 & 0 \\ 0 & 0 & 0 & 0 & 0 & 0 & 0 & 0 & 0 & 0 & 0 & 0 & 0 \\ 0 & 0 & 0 & 0 & 0 & 0 & 0 & 0 & 0 & 0 & 0 & 0 & 0 \\ 0 & 0 & 0 & 0 & 0 & 0 & 0 & 0 & 0 & 0 & 0 & 0 & 0 \\ 0 & 0 & 0 & 0 & 0 & 0 & 0 & 0 & 0 & 0 & 0 & 0 & 0 \\ 0 & 0 & 0 & 0 & 0 & 0 & 0 & 0 & 0 & 0 & 0 & 0 & 0 \\ 0 & 0 & 0 & 0 & 0 & 0 & 0 & 0 & 0 & 0 & 0 & 0 & 0 \\ 0 & 0 & 0 & 0 & 0 & 0 & 0 & 0 & 0 & 0 & 0 & 0 & 0 \\ 0 & 0 & 0 & 0 & 0 & 0 & 0 & 0 & 0 & 0 & 0 & 0 & 0 \\ 0 & 0 & 0 & 0 & 0 & 0 & 0 & 0 & 0 & 0 & 0 & 0 & 0 \\ 0 & 0 & 0 & 0 & 0 & 0 & 0 & 0 & 0 & 0 & 0 & 0 & 0 \\ 0 & 0 & 0 & 0 & 0 & 0 & 0 & 0 & 0 & 0 & 0 & 0 & 0 \end{pmatrix} \quad A_{31} = \begin{pmatrix} 0 & 0 & 0 & 0 & 0 & 0 & 0 & 0 & 0 & 0 & 0 & 0 & 0 \\ \frac{m_1 k_{as}}{\dot{m}_1} & 0 & 0 & 0 & 0 & 0 & 0 & 0 & 0 & 0 & 0 & 0 & 0 \\ 0 & 0 & 0 & 0 & 0 & 0 & 0 & 0 & 0 & 0 & 0 & 0 & 0 \\ 0 & 0 & 0 & 0 & 0 & 0 & 0 & 0 & 0 & 0 & 0 & 0 & 0 \\ 0 & 0 & 0 & 0 & 0 & 0 & 0 & 0 & 0 & 0 & 0 & 0 & 0 \\ 0 & 0 & 0 & 0 & 0 & 0 & 0 & 0 & 0 & 0 & 0 & 0 & 0 \\ 0 & 0 & 0 & 0 & 0 & 0 & 0 & 0 & 0 & 0 & 0 & 0 & 0 \\ 0 & 0 & 0 & 0 & 0 & 0 & 0 & 0 & 0 & 0 & 0 & 0 & 0 \\ 0 & 0 & 0 & 0 & 0 & 0 & 0 & 0 & 0 & 0 & 0 & 0 & 0 \\ 0 & 0 & 0 & 0 & 0 & 0 & 0 & 0 & 0 & 0 & 0 & 0 & 0 \\ 0 & 0 & 0 & 0 & 0 & 0 & 0 & 0 & 0 & 0 & 0 & 0 & 0 \\ 0 & 0 & 0 & 0 & 0 & 0 & 0 & 0 & 0 & 0 & 0 & 0 & 0 \\ 0 & 0 & 0 & 0 & 0 & 0 & 0 & 0 & 0 & 0 & 0 & 0 & 0 \end{pmatrix}$$

$$A_{24} = \begin{pmatrix} 0 & 0 & 0 & 0 \\ 0 & 0 & 0 & 0 \\ 0 & 0 & 0 & 0 \\ 0 & 0 & 0 & 0 \\ 0 & 0 & 0 & 0 \\ 0 & 0 & 0 & 0 \\ 0 & 0 & 0 & 0 \\ \frac{P_d A}{6\dot{m}_6} & 0 & 0 & 1-\frac{P_d A}{6\dot{m}_{10}} \\ \frac{P_d A}{6\dot{m}_6} & \frac{P_d A}{6\dot{m}_6} & 1-\frac{P_d A}{6\dot{m}_{10}} & -\left(1+\frac{P_d A}{6\dot{m}_{10}}\right) \\ 0 & 0 & 0 & 0 \\ 0 & 0 & 0 & 0 \\ 0 & 0 & 0 & 0 \\ 0 & 0 & 0 & 0 \end{pmatrix} \quad A_{35} = \begin{pmatrix} 0 & 0 & 0 & 0 \\ 0 & 0 & 0 & 0 \\ 0 & 0 & 0 & 0 \\ 0 & 0 & 0 & 0 \\ 0 & 0 & 0 & 0 \\ 0 & 0 & 0 & 0 \\ 0 & 0 & 0 & 0 \\ \frac{P_a A}{6\dot{m}_6} & 0 & 0 & 1-\frac{P_a A}{6\dot{m}_{10}} \\ \frac{P_a A}{6\dot{m}_6} & \frac{P_a A}{6\dot{m}_6} & 1-\frac{P_a A}{6\dot{m}_{10}} & -\left(1+\frac{P_a A}{6\dot{m}_{10}}\right) \\ 0 & 0 & 0 & 0 \\ 0 & 0 & 0 & 0 \\ 0 & 0 & 0 & 0 \\ 0 & 0 & 0 & 0 \end{pmatrix}$$

$$B = \begin{pmatrix} 0 & 0 & 0 & 0 & 0 & 0 & 0 & 0 & 1-\frac{P_d A}{6\dot{m}_{10}} & 0 & 0 & \frac{P_d A}{6\dot{m}_6} & 0 \\ 0 & 0 & 0 & 0 & 0 & 1-\frac{P_d A}{6\dot{m}_6} & 0 & 0 & 0 & \frac{P_d A}{6\dot{m}_{10}} & 0 & 0 & 0 \\ 0 & 0 & 0 & 0 & 0 & 0 & 0 & 0 & 0 & 0 & 0 & 0 & 0 \\ 0 & 0 & 0 & 0 & 0 & 0 & 0 & 0 & \frac{P_d A}{6\dot{m}_{10}} & 0 & 0 & -\left(1+\frac{P_d A}{6\dot{m}_6}\right) & 0 \\ 0 & 0 & 0 & 0 & 0 & 0 & 0 & 0 & 0 & 0 & 0 & 0 & 0 \\ 0 & 0 & 0 & 0 & 0 & 0 & 0 & 0 & 0 & 0 & 0 & 0 & 0 \\ 0 & 0 & 0 & 0 & 0 & 0 & 0 & 0 & 0 & 0 & 0 & 0 & 0 \\ 0 & 0 & 0 & 0 & 0 & 0 & 0 & 0 & 0 & 0 & 0 & 0 & 0 \end{pmatrix} \cdots$$

$$\cdots \begin{pmatrix} 0 & 0 & 0 & 0 & 0 & 0 & 0 & 0 & 0 & 0 & 0 & 0 & 0 \\ 0 & 0 & 0 & 0 & 0 & 0 & 0 & 0 & 0 & 0 & 0 & 0 & 0 \\ 0 & 0 & 0 & 0 & 0 & 0 & 0 & 0 & 0 & 0 & 0 & 0 & 0 \\ 0 & 0 & 0 & 0 & 0 & 0 & 0 & 0 & 0 & 0 & 0 & 0 & 0 \\ 0 & 0 & 0 & 0 & 0 & 0 & 0 & 0 & 1-\frac{P_a A}{6\dot{m}_{10}} & 0 & 0 & \frac{P_a A}{6\dot{m}_6} & 0 \\ 0 & 0 & 0 & 0 & 0 & 1-\frac{P_a A}{6\dot{m}_6} & 0 & 0 & 0 & \frac{P_a A}{6\dot{m}_{10}} & 0 & 0 & 0 \\ 0 & 0 & 0 & 0 & 0 & 0 & 0 & 0 & 0 & 0 & 0 & 0 & 0 \\ 0 & 0 & 0 & 0 & 0 & 0 & 0 & 0 & \frac{P_a A}{6\dot{m}_{10}} & 0 & 0 & -\left(1+\frac{P_a A}{6\dot{m}_6}\right) & 0 \end{pmatrix} \cdots$$

$$\cdots \begin{pmatrix} 0 & \frac{P_d A}{6\dot{m}_6} & -\left(1+\frac{P_d A}{6\dot{m}_{10}}\right) & 0 & 0 & 0 & 0 & 0 \\ -\left(1+\frac{P_d A}{6\dot{m}_6}\right) & 0 & 0 & \frac{P_d A}{6\dot{m}_{10}} & 0 & 0 & 0 & 0 \\ 1-\frac{P_d A}{6\dot{m}_6} & -\left(1+\frac{P_d A}{6\dot{m}_6}\right) & \frac{P_d A}{6\dot{m}_{10}} & \frac{P_d A}{6\dot{m}_{10}} & 0 & 0 & 0 & 0 \\ 0 & 1-\frac{P_d A}{6\dot{m}_6} & \frac{P_d A}{6\dot{m}_{10}} & 0 & 0 & 0 & 0 & 0 \\ 0 & 0 & 0 & 0 & 0 & \frac{P_a A}{6\dot{m}_6} & -\left(1+\frac{P_a A}{6\dot{m}_{10}}\right) & 0 \\ 0 & 0 & 0 & 0 & -\left(1+\frac{P_a A}{6\dot{m}_6}\right) & 0 & 0 & \frac{P_a A}{6\dot{m}_{10}} \\ 0 & 0 & 0 & 0 & 1-\frac{P_a A}{6\dot{m}_6} & -\left(1+\frac{P_a A}{6\dot{m}_6}\right) & \frac{P_a A}{6\dot{m}_{10}} & \frac{P_a A}{6\dot{m}_{10}} \\ 0 & 0 & 0 & 0 & 0 & 1-\frac{P_a A}{6\dot{m}_6} & \frac{P_a A}{6\dot{m}_{10}} & 0 \end{pmatrix}$$

$$s = \begin{pmatrix} \dot{s}_1 \\ \vdots \\ \dot{s}_{12} \\ \dot{s}_0 \end{pmatrix}, d = \begin{pmatrix} \dot{d}_1 \\ \vdots \\ \dot{d}_{12} \\ \dot{d}_0 \end{pmatrix}, a = \begin{pmatrix} \dot{a}_1 \\ \vdots \\ \dot{a}_{12} \\ \dot{a}_0 \end{pmatrix}, b = \begin{pmatrix} \dot{d}_{13} \\ \dot{d}_{14} \\ \dot{d}_{15} \\ \dot{d}_{16} \\ \dot{a}_{13} \\ \dot{a}_{14} \\ \dot{a}_{15} \\ \dot{a}_{16} \end{pmatrix}, s_0 = \begin{pmatrix} 0 \\ \vdots \\ 0 \\ \dot{s}_F \end{pmatrix}.$$

The solved model is attached as an Excel file to this TN.

4.2 Results of model calculations

4.2.1 SOLUTION OF MASS FLOW SYSTEM

The system is solved for an input mass flow $\dot{m}_0$ of 1L/h. 90% of the ingoing mass flow should leave the system as solid free nutrient liquid $\dot{m}_{11}$. 10% will go as highly concentrated particle stream to the *Fibrobacter* unit $\dot{m}_4$. The volume stream, which leaves the fermentor ($\dot{m}_1$) is ten times higher than the input mass flow $\dot{m}_0$. The mass flow through the RO-Unit $\dot{m}_8$ is set to 8 times the ingoing mass flow $\dot{m}_0$.

The solution yields the following mass flow vector and distribution coefficients.

$$\dot{m} = \begin{pmatrix} 10.00 \\ 3.567 \\ 6.433 \\ 0.100 \\ 6.333 \\ 2.667 \\ 0.900 \\ 8.000 \\ 7.100 \\ 7.100 \\ 0.900 \\ 2.667 \\ 1.000 \end{pmatrix} \qquad r = \begin{pmatrix} 0.64331 \\ 0.11250 \\ 0.01554 \\ 0.25232 \end{pmatrix}$$

4.2.2 SOLUTION OF THE SPECIES MASS FLOW SYSTEM

For a reactor volume of m_1=120L (HRT=5d), a specific membrane area of 25m²/m³ and permeability coefficients taken from the solution of the lab reactor system the following species mass flows were calculated in [g/h] resulting in the given concentrations [g/kg].

$$\dot{s} = \begin{pmatrix} 237.9 \\ 0.000 \\ 237.9 \\ 3.698 \\ 234.2 \\ 0.000 \\ 0.000 \\ 0.000 \\ 0.000 \\ 0.000 \\ 0.000 \\ 0.000 \\ 8.000 \end{pmatrix}, \dot{d} = \begin{pmatrix} 9.344 \\ 3.332 \\ 6.010 \\ 0.093 \\ 5.917 \\ 2.492 \\ 0.841 \\ 3.155 \\ 0.003 \\ 2.314 \\ 3.152 \\ 0.181 \\ 0.000 \end{pmatrix}, \dot{a} = \begin{pmatrix} 2.900 \\ 1.034 \\ 1.865 \\ 0.029 \\ 1.836 \\ 0.773 \\ 0.261 \\ 1.036 \\ 0.009 \\ 0.775 \\ 1.027 \\ 0.007 \\ 0.000 \end{pmatrix} \Leftrightarrow \quad s = \begin{pmatrix} 23.79 \\ 0.000 \\ 23.98 \\ 23.98 \\ 23.98 \\ 0.000 \\ 0.000 \\ 0.000 \\ 0.000 \\ 0.000 \\ 0.000 \\ 0.000 \\ 8.000 \end{pmatrix}, d = \begin{pmatrix} 0.934 \\ 0.934 \\ 0.934 \\ 0.934 \\ 0.934 \\ 0.934 \\ 0.934 \\ 0.394 \\ 4x10^{-4} \\ 0.326 \\ 3.502 \\ 0.067 \\ 0.000 \end{pmatrix}, a = \begin{pmatrix} 0.290 \\ 0.290 \\ 0.290 \\ 0.290 \\ 0.290 \\ 0.290 \\ 0.290 \\ 0.130 \\ 0.001 \\ 0.109 \\ 1.141 \\ 0.007 \\ 0.000 \end{pmatrix}$$

The calculated degradation of solid particles is 53.8%. 52.2% of the ingoing carbon leaves the system as nutrient steam. Just 1.6% of the carbon will enter the *fibrobacter* unit in a liquid state.

4.2.3 OPTIMIZATION OF VOLUME FLOWS

With the model parameter variations can be done to examine the impact of single parameters on the performance of the fermentor.
Two pumps will be necessary to maintain the circuit streams through the dialysate module. Higher flow rates will increase the mass transport performance of the module, while small volume flows will lead to very small concentration gradients and therefore reduced mass transport.
In figure 3 the mass flow leaving the fermentor $\dot{m}_1$ is modified.

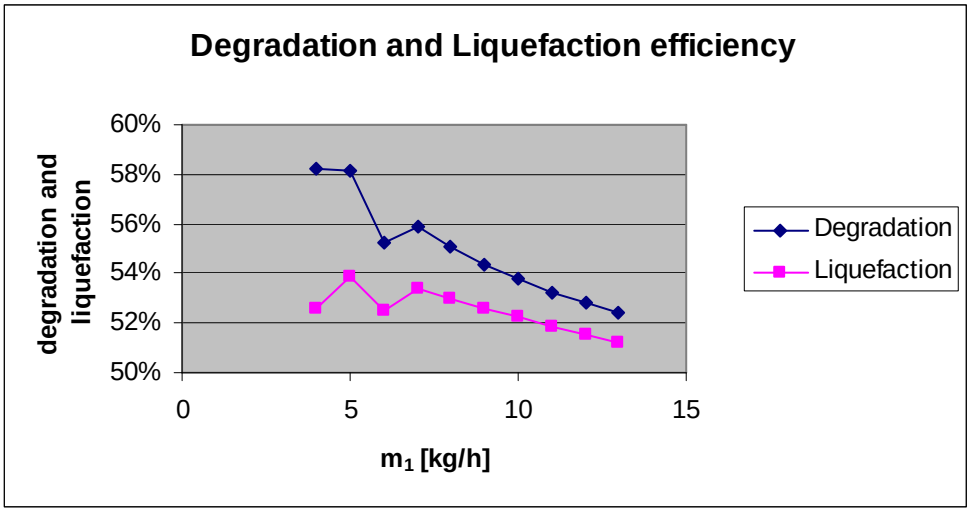

figure 5 Parameter variation of the mass flow m_1, impact on degradation and liquefaction. The liquefaction value is calculated from the amount of liquid carbon leaving the unit as concentrated nutrient stream. The degradation value is calculated from the amount of non degraded solids entering the *fibrobacter* unit. At lower mass flows the model becomes instable because of the linearization of the model.

Lower circuit streams will result in a higher degradation value. The reason for this is decrease of substrate in the fermentor with increasing volume flows as shown in figure 4.

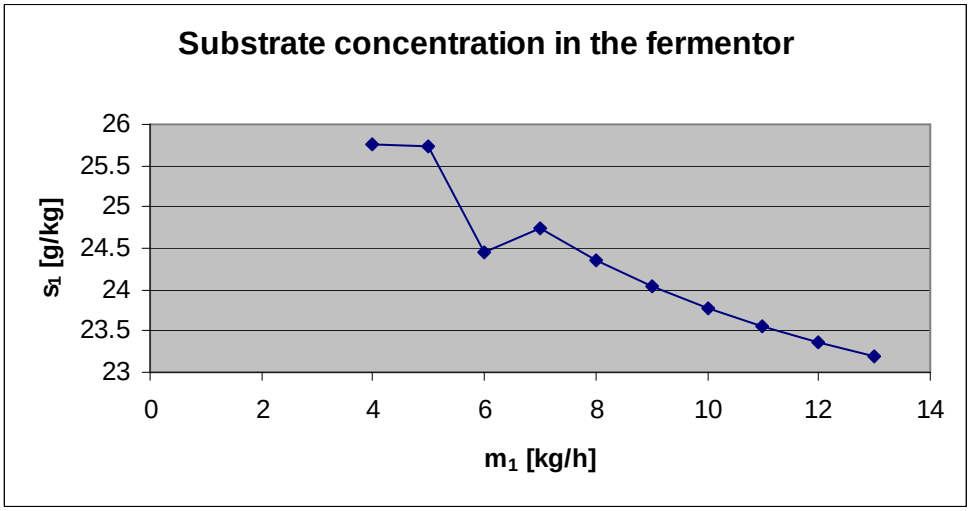

figure 6 solid substrate concentration in the fermentor. The concentration decreases with increasing volume flow leaving the fermentor. At low volume flows the linearized model becomes instable.

The second pump will cause the dialysate circuit to run. The pump will also raise the pressure above the osmotic pressure of the concentrated nutrient stream $\dot{m}_{11}$. The impact of the mass flow $\dot{m}_8$ onto the liquefaction and degradation performance is shown in figure 7.

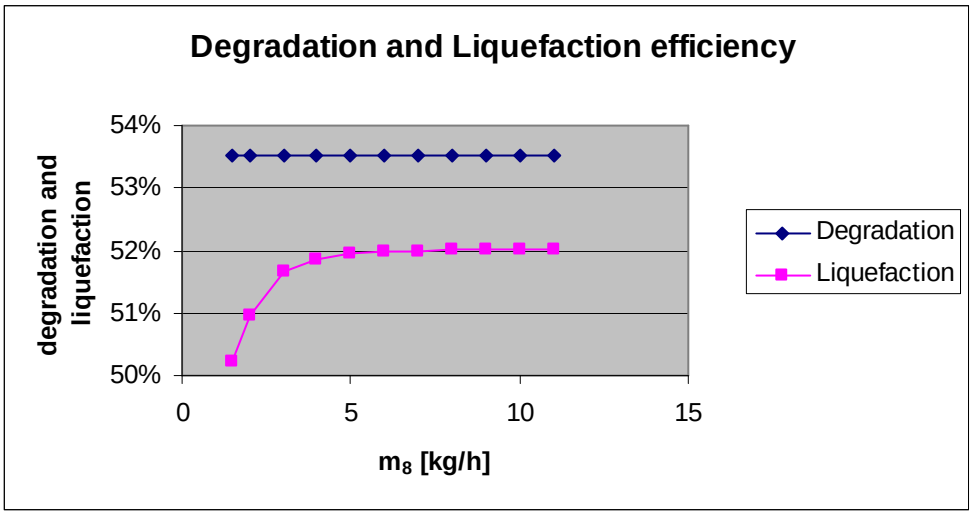

figure 7 Degradation and liquefaction efficiency of the hyperthermophilic liquefaction unit as a function of dialysate mass flow. The degradation is not effected by changes in the dialysate flow. The liquefaction will decrease at lower dialysate pump rates and more liquefied carbon will leave the system with the effluent to the *fibrobacter* unit.

A further increase of the dialysate pumping rate will not cause a better performance of the system. The pumping rate can be lowered to 4L/h without loosing much separation performance.

4.2.4 ENERGY REQUIREMENTS

The hyperthermophilic liquefaction unit will need thermal and mechanical energy. The thermal energy is needed to heat up the ingoing mass flow to 90°. Mechanical energy is required to operate the pumps.

4.2.4.1 Thermal energy demands

The thermal energy demands depend on the temperature of the environment T_e. The thermal energy will not be lost, but can be completely used to heat the space station, which maintains a higher temperature than the environment in space.
Mostly the heat can be regenerated by a heat exchanger. Figure 8 displays the connection.

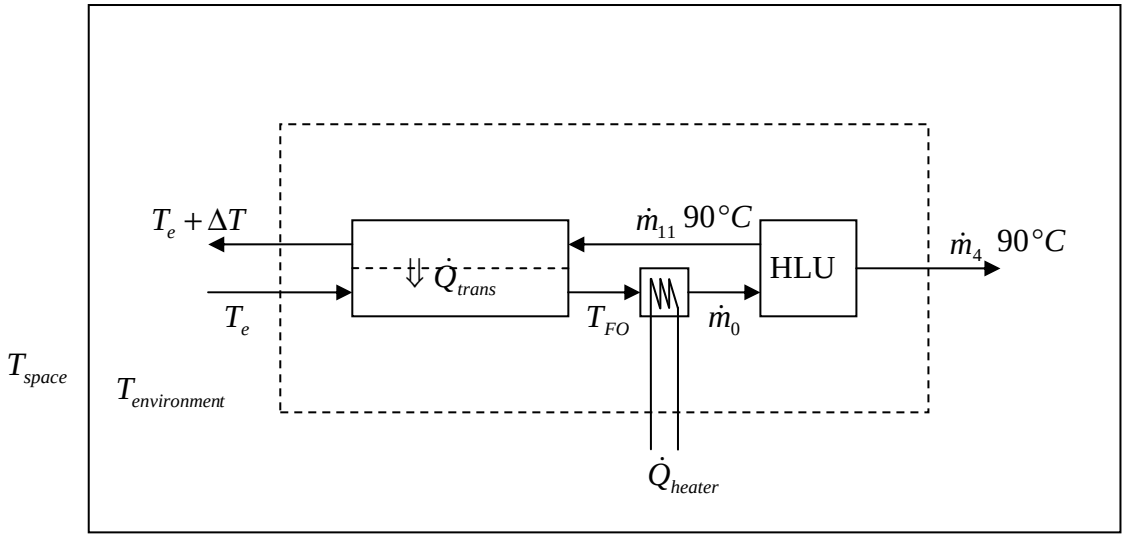

Figure 8 heat balance for the hyperthermophilic liquefaction unit. The effluent can be used to heat up the feed stream.

A large heat exchanger will cause a very small temperature gradient ΔT. Smaller heat exchangers will lead to reduced weight, but higher thermal energy demands, as the temperature of the effluent rises. The heat balance is written in eq. 26. The reference temperature T_{ref} can be set to an arbitrary value. It is needed to formulate the heat balance correctly.

$$\dot{m}_0 \cdot c_p \cdot (T_e - T_{ref}) + \dot{Q} = \dot{m}_4 \cdot c_p \cdot (90°C_e - T_{ref}) + \dot{m}_{11} \cdot c_p \cdot (T_e + \Delta T - T_{ref}) \qquad \text{(eq.26)}$$

The heat loss is therefore eq.27

$$\dot{Q} = c_p \cdot (\dot{m}_4 \cdot 90°C + \dot{m}_{11} \cdot (T_e + \Delta T) - \dot{m}_0 \cdot T_e) + T_{ref} \cdot c_p \cdot \underbrace{(\dot{m}_0 - \dot{m}_{11} - \dot{m}_4)}_{0} \qquad \text{(eq.27)}$$

A temperature gradient has to be chosen because which offers the best combination of investment and process costs.
The heat loss is direct proportional to ΔT. (eq.28).

$$HL = c_p \cdot \Delta T \cdot \dot{m}_{11} \quad \text{(eq.28)}$$

The heat exchanger size increases with the heat exchanger area to the power of (3/2). The heat exchanger area can be written according to eq.29.

$$A = \frac{\dot{Q}_{trans}}{\Delta_{\log} T \cdot k} \quad \text{(eq.29)}$$

The temperature at the feed outlet is calculated with a heat balance over the heater.(eq.30)

$$T_{FO} = 90°C - \frac{\dot{Q}_{heater}}{c_p \cdot \dot{m}_0} \quad \text{(eq.30)}$$

The average logarithmic temperature difference is shown in eq.31.

$$\Delta_{\log} T = \frac{\Delta T - (90°C - T_{FO})}{\ln\left(\frac{\Delta T}{(90°C - T_{FO})}\right)} \quad \text{(eq.31)}$$

The heat exchanger size is computed by combining eq.29-31 to eq.32.

$$V = \left(\frac{\dot{m}_0 \cdot c_p \cdot (T_{FO} - T_e)}{\Delta_{\log} T \cdot k}\right)^{\left(\frac{3}{2}\right)} \quad \text{(eq.32)}$$

Heat loss and heat exchanger volume normalized for a temperature gradient of 10°C and shown in Figure 9

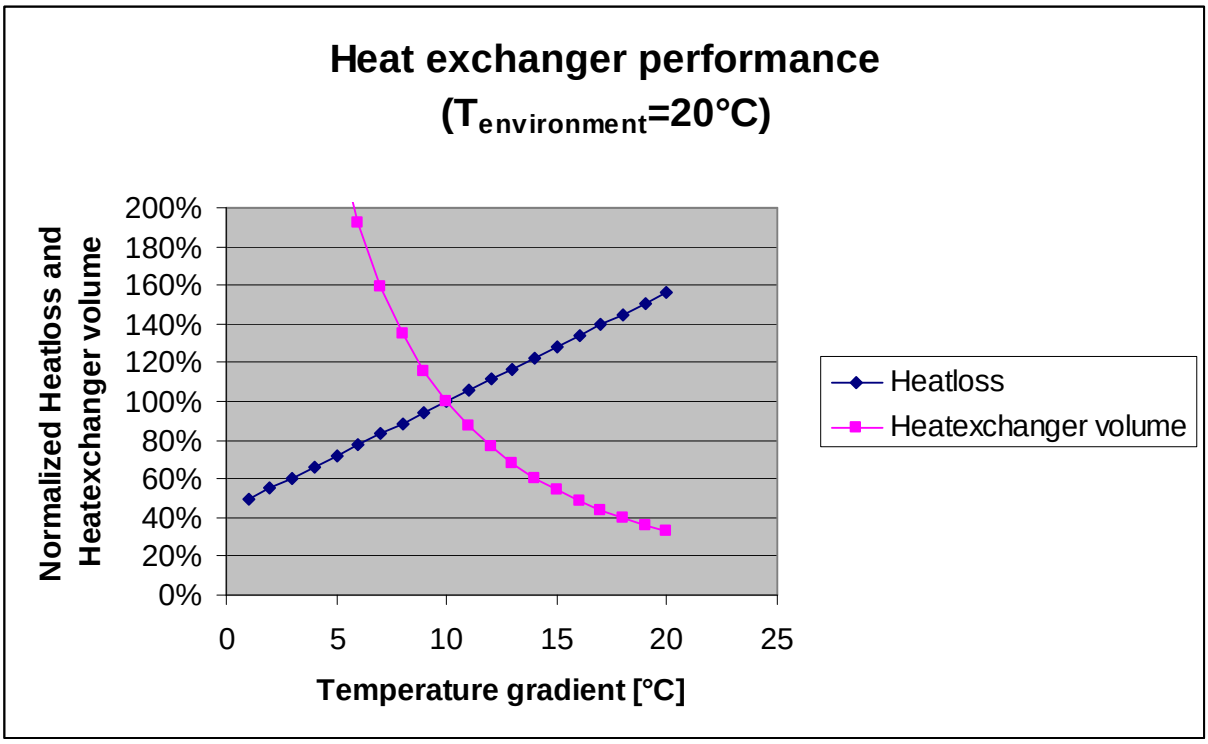

Figure 9 Heat exchanger performance for $T_{fermentor}$=90°C, $T_{environment}$=20°C, m_{11}=0.9xm_0. The values are normalized for ΔT=10°C. An increase of ΔT from 10°C to 15°C will lead to a 30% higher heat loss but to a 45% lower heat exchanger volume.

With a temperature gradient of ΔT=15 °C the heat demand of the system is calculated to

$$\dot{Q}_{heater} = 23.7\frac{W}{L}$$

4.2.4.2 Mechanical energy demand

Four pumps are needed for the system. The first pump will drive the feed ($\dot{m}_0$) into the fermentor. An average pressure of 0.5bar seems feasible. The second pump drains the fermentor ($\dot{m}_1$) and builds up the pressure necessary for the MF. Normally MF modules are run with a trans-membrane pressure of maximal 2 bars [3]. The third pump is required to build up the pressure for the RO-Unit ($\dot{m}_8$). The pressure can be calculated with van't Hoffs Equation (eq.33). The last pump is needed to overcome the pressure drop in the dialysate module ($\dot{m}_6$). A pressure drop of 0.5 bar should not be exceeded, otherwise a convective mass flow can be observed.

$$\Pi = RT \cdot c \qquad \text{(eq.33)}$$

Π is the osmotic pressure, R the Gas-constant, c the concentration of small molecules in the permeate, T the absolute temperature. The osmotic pressure is calculated to 0.53bar.
The impact of pressure on the specific enthalpy of water at 90°C can be computed with eq.34.

$$\left.\frac{dh}{dp}\right|_{T=90°C} = 0{,}0774\frac{kJ}{kg \cdot bar} \qquad \text{(eq.34)}$$

The mechanical energy demand of the hyperthermophilic liquefaction unit sums up to eq.35.

$$\dot{W}_{mech} = \frac{dh}{dp} \cdot \left(\dot{m}_0 \cdot 0.5bar + \dot{m}_2 \cdot 1.5bar + \dot{m}_6 \cdot 0.5bar + \dot{m}_8 \cdot 0.53bar\right) \qquad \text{(eq.35)}$$

For one liter per hour of wastewater a mechanical energy supply of 0.43W is needed.

5 CONCLUSIONS

The hyperthermophilic liquefaction unit can provide other compartments in the MELiSSA loop with concentrated and easy degradable nutrient stream. In the nutrient no toxic substances like aromatic or halogenated molecules were detected. The nutrient stream consists largely of proteins and carbohydrates with smaller amounts of volatile fatty acids, amino acids and reducing sugars.
A simple model was developed to describe the degradation of solid particles to dissolved organic carbon and volatile fatty acids. The reaction is modeled with a first order reaction. The obtained parameters seem logical and within the expected boundaries.
The reaction rate constants were needed for an enhanced model, which describes the scale up of the system. Due to stability reasons the laboratory set up can not be up scaled by expanding the geometrical dimensions. A dialysate module has to be applied and combined with a Reverse osmosis unit to remove the liquefied products.
The prediction of the behavior of coupled systems is not an easy task. Often the complete system has to be solved to examine the answer of one variable to the change of another one. The introduction of a counter current dialysate module brought in non-linearities. This could be circumvented by linearizing the average concentration gradient. The dialysate module was split into three separate partitions. For each partition the gradient was linearized.
The approach works for small to medium specific membrane areas. Bigger membrane modules will need a greater number of intersections for a correct calculation.
With the linear model parameter studies were done. It was shown that the dialysate stream could be severely reduced to certain levels without limiting the liquefaction performance.
The heat and energy demands were calculated. For heating approx. 23.7kW/($m^3\ h^{-1}$) are needed. Electrical energy for pumps has to be supplied for 450W/($m^3\ h^{-1}$).
It has to be considered that the heating energy is not “gone” but will help to maintain the space station at the working temperature which is normally much higher than environmental temperature in space.

Literature:

[1] Himmel, Baker, Overend. Enzymatic conversation of Biomass for fuels production. American Chemical Society Symposium series 566. 1994 pp 419-422

[2] Thomas, Alexander. Microbial Formation of Secondary and Tertiary Amines in Municipal Sewage. Appl environ microbiol, Sept. 1981, p. 461-463

[3] Mulder. Basic principles of Membrane Technology. Second edition. 1998 Kluwer Academic Publishers p287

Appendix: Compounds Identified in Biomass Extracts and pretreatment Hydrolyzates [1]

Acids	Alcoholes	Aldehydes
Acetic acid	Coniferyl alcohol	Cinnamaldehyde
Capronic acid	Dihydroconiferyl alcohol	Coniferyl aldehyde
Caprylic acid	Dihydrosinapyl alcohol	Furfural
Cinnamic acid	3,5-dimetoxy-4-4hydroxycinnamyl	p-hydroxybenzaldehyde
Coumaric acid	b-oxysinapyl alcohol	p-hydroxycinnamaldehyde
Formic acid	Sinapyl alcohol	5-Hydroxymethylfurfural
Glucuronic acid	1-Syringylacetol	Sinapaldehyde
Galacturonic acid	Syringyl glycerol	Sinapyl aldehyde
m-Hydroxybenzoic acid		Syringaldehyde
p-Hydroxybenzoic acid		Vanillin
Levulinic acid		
Pelargonic acid		
Palmitic acid		
Syringic acid		
Syringylglycolic acid		
Vanillic acid		